Adsorption of 12− s −12 Gemini Surfactants at the Silica−Aqueous Solution Interface

ARTICLE *in* THE JOURNAL OF PHYSICAL CHEMISTRY B · APRIL 2003

Impact Factor: 3.3 · DOI: 10.1021/jp026626o

4 AUTHORS:

Rob Atkin
University of Newcastle
106 PUBLICATIONS **3,624** CITATIONS
SEE PROFILE

Vincent S J Craig
Australian National University
101 PUBLICATIONS **4,037** CITATIONS
SEE PROFILE

Erica J Wanless
University of Newcastle
81 PUBLICATIONS **2,511** CITATIONS
SEE PROFILE

Simon Richard Biggs
University of Queensland
235 PUBLICATIONS **5,306** CITATIONS
SEE PROFILE

Adsorption of 12-*s*-12 Gemini Surfactants at the Silica−Aqueous Solution Interface

R. Atkin,[†,§] V. S. J. Craig,[‡] E. J. Wanless,*[,†] and S. Biggs[†,||]

Discipline of Chemistry, School of Environmental and Life Sciences, The University of Newcastle, Callaghan NSW 2308, Australia, and Department of Applied Mathematics, Research School of Physical Sciences and Engineering, Australian National University, Canberra ACT 0200, Australia

Received: July 28, 2002; In Final Form: January 9, 2003

The adsorption of gemini surfactants of the form alkanediyl-α,ω-bis (dodecyldimethylammonium bromide) to a silica substrate is investigated using optical reflectometry (OR) and atomic force microscopy (AFM). The adsorption isotherms and kinetics of adsorption have been determined for spacer sizes of 2, 3, 4, 6, 8, 10, and 12. The maximum surface excess correlates strongly with the size of the spacer group. The smallest spacer size yields the largest surface excess. Soft-contact AFM imaging has shown that flattened ellipsoidal aggregates are present on the surface at the shortest spacer lengths. Images of the adsorbed layer cannot be obtained for spacer sizes greater than 3 because of a strongly attractive force regime. The origin of the attraction is attributed to proximal desorption induced by the approach of the tip toward the substrate. The linear increase in the area per adsorbed molecule with spacer size suggests that the aggregate structures become flattened with increasing spacer size but are otherwise similar.

Introduction

Gemini surfactants are a relatively new class of amphiphilic molecules, first appearing in the literature in 1974.[1] They have become a topic of scientific interest due in part to their effectiveness in the modification of interfacial properties but also because their molecular geometries lead to interesting aggregate structures both in solution and at the solid−aqueous interface.[2,3]

A gemini surfactant consists of two surfactant molecules joined by an alkyl spacer group. The surfactant molecules are often identical. The spacer group can be flexible or rigid,[4] hydrophilic or hydrophobic,[5] and it generally connects the two surfactant moieties at, or near, the headgroup. The attachment of the spacer group increases the hydrophobicity of the dimeric surfactant relative to that of the constituent monomeric units. As a consequence, the cmc of the gemini surfactant can be up to 100 times lower than that of the monomeric analogue.[6] For simplicity, shorthand nomenclature for gemini surfactants, which is based on the number of carbon atoms in the surfactant chain (m) and the spacer group (s), is often employed and is best illustrated by example. For alkanediyl-α,ω-bis (dodecyldimethyl-ammonium bromide) dimeric surfactants with the alkanediyl spacer groups C_2H_4 or C_8H_{20}, the corresponding surfactants are referred to as 12-2-12, and 12-8-12, respectively. This paper is concerned only with 12-*s*-12 surfactants.

The properties of gemini surfactants are greatly influenced by the length of the spacer group. The spacer group controls the separation between the headgroups that may be greater or less than the average separation of the corresponding monomer in an aggregate. This changes the mobility and the packing geometry of the surfactant within an aggregate, whether in solution or at a surface. Danino et al.[7] have demonstrated that the structure of the micelles formed in solution varies significantly with spacer length. For quaternary ammonium surfactants of the form 12-*s*-12, for $s \leq 5$ the headgroups are in close proximity. The Bjerrum length in water at 25 °C is 0.7 nm.[8] Therefore, gemini surfactants with short spacer lengths will have a charge of less than 2, as charge condensation must occur. The smaller headgroup area leads to aggregates of lower curvature than that of the corresponding monomer for low *s* values. For $6 \leq s \leq 12$, the distance between headgroups induced by the spacer is similar to that of the monomer, and similar aggregate structures result. For $s > 14$, the spacer adopts a looped conformation within the aggregate, effectively increasing the hydrocarbon chain volume. The structure formed in this case is similar to those of dimeric surfactants.[7,9−11]

The effect of the length of the spacer group on adsorption at the solution−air interface has been extensively investigated. It has been demonstrated that the surface area occupied per surfactant molecule increases with the size of the spacer for $3 \leq s \leq 10$. The behavior of gemini surfactants at the solid−liquid interface has been shown to follow similar trends.[12,13] The adsorption of 12-2-12 was investigated at the silica−aqueous interface,[14] the Laponite clay−aqueous interface,[15] and the titanium−aqueous interface.[16] It was shown that the maximum surface excess of 12-2-12 at the silica−aqueous interface was lower than that of the monomeric analogue, DTAB.

Chorro et al.[17] have shown using electrophoretic measurements that at low surfactant concentrations the silica is substantially negatively charged as adsorption begins, and the surface excess in terms of molecules per unit area at the point of zero charge was the same irrespective of the spacer length. The area occupied per surfactant molecule is 25 nm^2 at the pzc, and this equates to an average distance between monomers of 5 nm. This distance is much larger than the length of a fully extended spacer group (about 1.4 nm for 12-10-12). Therefore,

* Corresponding author. E-mail: ewanless@mail.newcastle.edu.au.
† The University of Newcastle.
‡ Australian National University.
§ Current address: School of Chemistry, University of Bristol, Cantock's Close, Bristol, BS8 1TS, U.K.
|| Current address: School of Process, Environmental and Materials Engineering, University of Leeds, Leeds, LS2 9JT, U.K.

10.1021/jp026626o CCC: $25.00
Published on Web 00/00/0000 PAGE EST: 7.9

TABLE 1: Characteristics of Investigated Gemini Surfactants

surfactant name	structural formula	abbreviation	aggregate structure in solution[7,9−11]	cmc (mM)[25]	α[26]
ethyl-α,ω-bis(dodecyldimethyl-ammonium bromide)	$C_2H_4(C_{12}H_{25}N^+Me_2\ Br^-)_2$	12-2-12	wormlike	0.84	0.15
propyl-α,ω-bisdodecyldimethyl-ammonium bromide)	$C_3H_6(C_{12}H_{25}N^+Me_2\ Br^-)_2$	12-3-12	extended micelles	0.87	0.16
butyl-α,ω-bis(dodecyldimethyl-ammonium bromide)	$C_4H_8(C_{12}H_{25}N^+Me_2\ Br^-)_2$	12-4-12	spherical micelles	1.09	0.15
hexyl-α,ω-bis(dodecyldimethyl-ammonium bromide)	$C_6H_{12}(C_{12}H_{25}N^+Me_2\ Br^-)_2$	12-6-12	spherical micelles	1.01	0.20
octyl-α,ω-bis(dodecyldimethyl-ammonium bromide)	$C_8H_{16}(C_{12}H_{25}N^+Me_2\ Br^-)_2$	12-8-12	spherical micelles	0.83	0.25
decyl-α,ω-bis(dodecyldimethyl-ammonium bromide)	$C_{10}H_{20}(C_{12}H_{25}N^+Me_2\ Br^-)_2$	12-10-12	spherical micelles	0.63	0.25
dodecyl-α,ω-bis(dodecyldimethyl-ammonium bromide)	$C_{12}H_{24}(C_{12}H_{25}N^+Me_2\ Br^-)_2$	12-12-12	spherical micelles	0.37	0.31

one surfactant can neutralize only one surface-charge site. At surfactant concentrations above the cmc, it was shown that as the size of the spacer group increased the maximum surface excess of surfactant decreased,[17] an effect that was attributed to an increased headgroup area altering the structure of the adsorbed aggregate. However, in the absence of direct evidence of the adsorbed surfactant structure, this interpretation cannot be confirmed.

The current study aims to elucidate the relationship between spacer length and surface adsorbate morphology. Although the geometry of gemini surfactants is quite different from that of similar monomeric surfactants, it has been suggested[17,18] that the adsorption mechanism of gemini surfactants has features in common with that of conventional surfactants. In view of this, we shall briefly review current views on the adsorption of cationic surfactants to silica.

The adsorption process for cationic surfactants on silica[19−21] involves three fundamental stages, which divide the isotherm into four zones. In the first stage, surfactants are electrostatically adsorbed to the charged surface sites. The presence of the positively charged headgroup at the interface renders nearby hydroxyl groups more acidic, inducing more charged sites in the vicinity of the initial surface charge.[19] The surfactant tail may interact with hydrophobic regions on the substrate if any are present. The hydrophobic tail of the surfactant and the newly induced surface sites now act as nucleation points for further surfactant adsorption. This is the second stage in the adsorption process and is driven by hydrophobic interactions and electrostatic attraction. Throughout the second stage, the charge on the underlying surface continues to increase. At the end of stage two, the adsorbed morphology is known as a "tepee" structure, and the substrate ionization is a maximum. Any further adsorption is purely hydrophobically driven and is against an electrostatic barrier that is present because of overcompensation of the surface charge by the surfactant already present. Stage three is characterized by the hydrophobic adsorption of surfactant molecules to the tepees already adsorbed at the interface, with headgroups oriented away from the surface. In stage three, the level of counterion adsorption becomes appreciable, and surfactant continues to accumulate in the existing adsorbed aggregates or admicelles until a maximum in adsorption is reached, denoting the beginning of stage four.[21] Further increases in the bulk surfactant concentration have no effect on the surface excess.

Investigating surfactant adsorption at the solid−aqueous interface poses unique difficulties. Despite the contribution of several studies, a complete picture of gemini surfactant adsorption at the solid−aqueous interface is yet to emerge. To quantify the surfactant adsorption process at the solid-aqueous interface completely, the equilibrium surface excess must be equated with the structure of the adsorbed surfactant layer, and the adsorption mechanism must be determined. The equilibrium surface excess at any surfactant concentration can be determined using a variety of traditional[17−20] and ellipsometric techniques.[22,23] In both instances, the most common substrate used is amorphous silica in the form of silica particles or oxidized, polished silicon wafers. Although this is not problematic in itself, the majority of the information concerning the adsorbed morphology of surfactant aggregates is derived from data acquired using AFM.[24] As the AFM is particularly well suited to detecting the periodicity of discrete surface aggregates, AFM images of adsorbed surfactant layers are obtained most readily on crystalline substrates that strongly template the adsorbing surfactant into regularly arranged structures. Obtaining AFM images on amorphous silica is more difficult because of increased disorder both within the aggregates and in their arrangement at the surface. Thus, the majority of AFM studies concerning surfactant adsorption have been reported on atomically smooth, strongly templating substrates such as graphite and mica. This is particularly true for gemini surfactants, where the only reported adsorbed morphologies are hemimicellar and cylindrical structures on graphite and mica,[2] respectively. The use of different substrates precludes a direct comparison between information obtained using different methods. On substrates where images of the adsorbed aggregate structures are readily obtained, there is no corresponding adsorption isotherm data. Conversely, adsorption isotherm studies at the silica−aqueous interface for gemini surfactants have dealt with amorphous silica,[17] where images of the structure of the adsorbed aggregate have not been reported. Therefore, the morphology of structures formed in solution and on other substrates is used, along with adsorption isotherms, to imply the adsorbed aggregate structure. The current study aims to overcome this disparity.

Materials and Methods

The gemini surfactants utilized in this study were kindly provided by Professor Raoul Zana and were used without further purification. The solution cmc values, micelle ionization degree, and solution aggregate morphology for the surfactants used are provided in Table 1. All water used was filtered, distilled, and passed through a Millipore filtration unit before use. Silicon wafers were baked at 1000 °C for 100 min in an oxygen atmosphere to produce an oxide layer (SiO_2). Hydroxylated silica was prepared by soaking pyrogenic silica in water for 48 h followed by treatment with 10 wt % NaOH for 30 s and rinsing in water and then ethanol before drying under a

nitrogen stream. The thickness of the oxide layer present on the silicon wafer was determined ellipsometrically using an Auto EL-II automatic ellipsometer (Rudolf Research) to be 165 ± 1 nm for both the hydroxylated and pyrogenic silicas. The refractive indices of silica and silicon used in the determination of the surface excess were 1.46 and 3.8, respectively. These wafers were used as the substrates for both optical reflectometry and AFM adsorption studies.

The optical reflectometry technique used to measure surface excess concentrations follows that described by Dijt et al.[27] and has been described in detail in a previous paper.[23] Briefly, reflectometry relies upon determining the change in the polarization of light reflected from the substrate during adsorption. In a typical reflectometry experiment, the cell initially contains pure water, and a stable baseline is recorded. Surfactant is then passed into the cell, and the change in the ratio of the s and p polarizations of the reflected laser beam is recorded. This is proportional to the surface excess. The proportionality is determined using an appropriate optical model that requires the refractive indices of the solvent, silica, and silicon to be known as well as the thickness of the silica layer and the refractive index increment (dn/dC) of the adsorbing solution. The values of dn/dC used in this study were determined using a Wyatt differential refractometer. The dn/dC values were between $0.1649 \pm 5 \times 10^{-4}$ and $0.1747 \pm 6 \times 10^{-4}$ for all spacer sizes. The optical reflectometer is entirely contained in an incubator, allowing the temperature to be accurately maintained at 25.0 ± 0.1 °C.

AFM images of adsorbed surfactant structures were obtained using a Nanoscope III AFM (Veeco Metrology) operating in the "soft-contact" mode as described previously.[28,29] Silicon nitride cantilevers from Olympus were used. These had sharpened tips with a radius of less than 20 nm and a spring constant of ∼0.09 Nm^{-1}. The image presented in the current study is a deflection image obtained at a scan rate of 10 Hz with integral and proportional gains between 1 and 3. Force curves and substrate images were first obtained in water to ensure that the surfaces were clean. Surfactant solutions were then introduced into the cell, and images of the surface were taken after elapsed times of between 5 min and 24 h. The AFM was contained in an incubator, allowing the temperature to be accurately maintained at 25.0 ± 0.1 °C.

Results

A comparison of adsorption studies on silica, particularly those undertaken using different techniques, can be complicated by the variability in the properties of the substrate with the methods employed to clean and prepare the surface.[18,23,30−32] In this study, the silicon wafers used in both optical reflectometry and AFM were derived from the same silicon wafer and have been prepared under identical conditions. This permits direct comparison between the surface excess and adsorbed layer morphology.

The adsorption of 12-s-12 gemini surfactants to silica as a function of time is presented in Figure 1. The surfactant concentrations shown are approximately 1 × cmc. For a given spacer length, there was no variation in the form of the data over the range of surfactant concentrations studied. For each surfactant, a baseline was obtained for ∼15 s prior to surfactant being introduced into the cell, at which time the surface excess rapidly increases. For all spacer lengths, equilibrium adsorption levels are attained within 4 s of adsorption commencing. The surface excess rises rapidly to approximately 70% of the equilibrium surface excess followed by a slower increase to the final value. The equilibrium surface excess remained constant while the surfactant concentration was maintained. For comparison, the adsorption curve of CTAB, also at 1 × cmc, is included. CTAB has a longer alkyl chain (C_{16}) than the gemini surfactants under investigation here but a similar cmc (0.9 mM) and therefore provides an appropriate comparison. The form of the adsorption for CTAB is similar to that of the gemini surfactants and identical to that obtained for 12-3-12. Upon water being passed into the cell, desorption was complete and rapid for all surfactants (not shown).

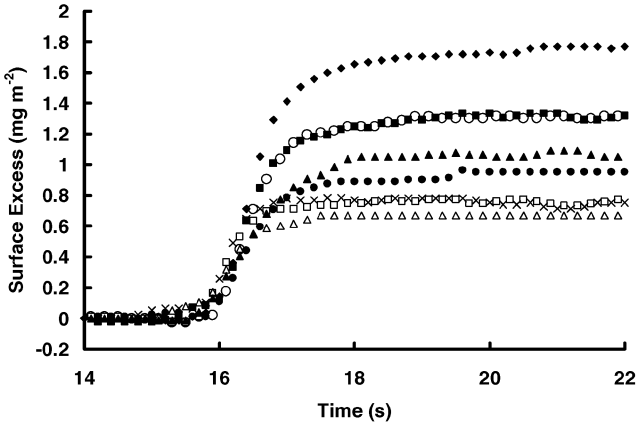

Figure 1. Sample data for the adsorption of 12-s-12 gemini surfactants at the silica−solution interface at a concentration of 1 × cmc: 12-2-12 (♦), 12-3-12 (■), 12-4-12 (▲), 12-6-12 (●), 12-8-12 (□), 12-10-12 (×), and 12-12-12 (△). A typical adsorption result for 1 mM CTAB (○) is included for comparison. The surfactant solution is first passed into the cell at ∼15.5 s, leading to surfactant adsorption. The plateau level of adsorption is maintained while the surfactant solution is flowing into the cell.

Several previous studies have reported adsorption isotherms for gemini surfactants on particulate silica by the solution depletion method. This method has some limitations. The surface charge of the silica substrate varies not only with pH but also with surfactant adsorption.[19,20] Therefore, in depletion experiments with a high surface-to-volume ratio, the ionic strength of the supernatant can vary along an isotherm, complicating the interpretation. This is further compounded by the release of metal ions, particularly sodium, from the particulate silica. More recent studies have attempted to overcome this difficulty by acid-washing the silica prior to adsorption, with some degree of success. However, acid-washing the substrate will alter the surface chemistry of the substrate appreciably.[33] These difficulties have been overcome in the current study. The silica wafers used in this investigation are of high purity and do not possess significant levels of metal ions. Additionally, adsorption measurements obtained using optical reflectometry are under constant flow, and the surface area under investigation is small so that any H^+ ions released from the substrate will be quickly removed from the reflectometry cell. Therefore, the solution conditions are unaffected by the adsorption of the surfactant to the substrate. The major disadvantage of reflectometry compared with solution depletion studies is the relatively high detection limit of the instrument (on the order of 0.025 mg m^{-2}), making it generally unsuitable for the study of the first adsorption stage (charge neutralization).[21]

Adsorption isotherms are presented in Figure 2 for the spacer lengths investigated here, with the concentration axis normalized by the solution cmc. Below 0.3 × cmc, the adsorption isotherms are apparently coincident. This indicates that electrostatic interactions between the substrate and the adsorbed surfactant play a dominant role in the adsorption process up to this

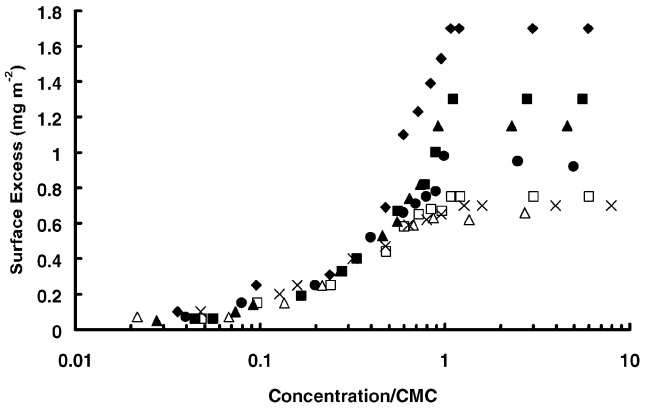

Figure 2. Adsorption isotherms for 12-*s*-12 gemini surfactants at the silica−solution interface with the concentration axis as a function of the cmc: 12-2-12 (♦), 12-3-12 (■), 12-4-12 (▲), 12-6-12 (●), 12-8-12 (□), 12-10-12 (×), and 12-12-12 (△). Below 0.3 × cmc, there is no apparent variation in the surface excess with spacer size. Above 0.3 × cmc, the isotherms begin to separate, and the saturation surface excess decreases with increasing spacer size.

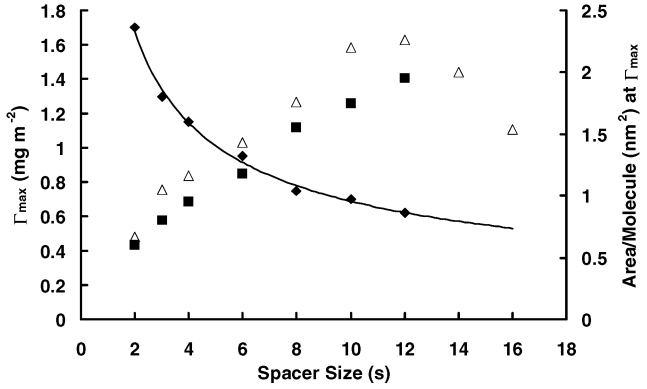

Figure 3. Variation in the saturation surface excess, Γ_{max}, (♦) and the area per adsorbed molecule at Γ_{max} (■) with spacer length. For comparison, the area per molecule at the air−water interface (△) determined by Espert et al.[12] and Alami et al.[13] is presented. This provides a measure of the area per molecule in a fully formed monolayer. Optical reflectometry measures a combination of the change in the refractive index and thickness of an adsorbed layer and cannot distinguish between counterions in solution and those associated with a headgroup. Thus, all counterions contribute to the change in the refractive index that is used to calculate the adsorbed mass. As a consequence, all counterions are included in the calculation that converts an adsorbed mass to a molecular density.

concentration. At higher concentrations, surfactants with shorter spacer lengths have greater surface excess values. The highest surface excess value obtained is the saturation value for that surfactant, Γ_{max}. Adsorption at these concentrations is hydrophobically driven and takes place against an electrostatic barrier. For all spacer lengths, the saturation surface excess is reached at or slightly below the solution cmc, with no increase in surface excess detectable up to 10 × cmc.

The variation in Γ_{max} with spacer length is presented in Figure 3. As previously reported, the value of Γ_{max} decreases with increasing spacer length.[17] These data are easily converted to the area per adsorbed molecule assuming single-layer coverage and two adsorbed counterions at Γ_{max}, which is also presented in Figure 3. Note that the counterions will largely be in close proximity to the adsorbed molecules and therefore will contribute to the surface excess as measured by optical reflectometry. The area per adsorbed molecule increases in a linear fashion with spacer length for the spacer sizes investigated here. Some insight into the adsorbed morphology can be obtained

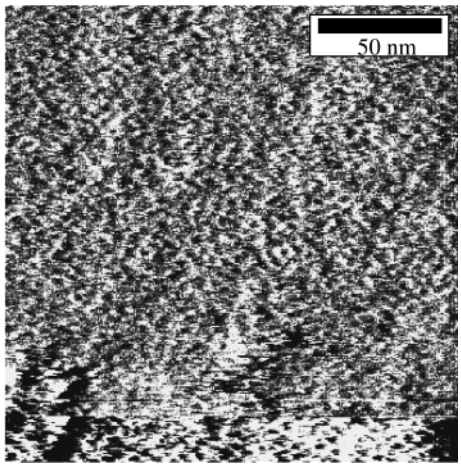

Figure 4. AFM image of the silica−solution interface immersed in an aqueous solution of 2 × cmc 12-2-12 revealing adsorbed aggregates with approximately circular profiles in the upper portion of the image. The slow scan direction is down the page. The underlying silica surface is seen in the lower portion of the image when a higher imaging force is applied.

by comparing the area per molecule at the silica−water interface to that obtained at the air−water interface, where a monolayer adsorbed structure is well established. In view of this, area per molecule data at the air−water interface determined in the studies of Espert et al.[12] and Alami et al.[13] are presented for comparison. By halving the area per molecule at the air−water interface, an approximation of the area per molecule in a fully formed bilayer is obtained. For all spacer lengths investigated in this study, the area per adsorbed molecule at the silica−water interface is greater than that for a fully formed bilayer. This suggests the formation of discrete bilayered surface aggregates.

Images of the adsorbed surfactant morphology at the solid−liquid interface can be obtained using direct in-situ AFM. An image of the hydroxylated silica−solution interface immersed in an aqueous solution of 12-2-12 at ∼2 × cmc is presented in Figure 4. Adsorbed flattened ellipsoidal structures are observed on the silica surface with an adsorbed layer thickness of 3.5 ± 0.2 nm and an average peak-to-peak distance of the adsorbed aggregates of 8.0 ± 0.5 nm. The adsorption density was found to be 150 aggregates per 10 000 nm^2. No discernible change in structure was observed in the images collected regularly over 6 h. Similar aggregate structures were imaged for $s = 3$. However, for $s \geq 4$, images of adsorbed structures could not be obtained because the imaging tip was attracted to the surface from separations >9 nm. That is, the necessary conditions for soft-contact imaging were not present.

The deflection force curve can provide both quantitative and qualitative data with regard to the structure of the adsorbed gemini surfactant layer. Force versus distance plots are presented in Figures 5 and 6 for 12-2-12 and 12-12-12, respectively The insets show the same data presented on a log−linear scale and fitted using the DLVO theory and constant potential boundary conditions. Force curves obtained in the presence of 12-3-12 were of a similar form to those obtained with 12-2-12, and the force curves presented for 12-12-12 are representative of force curves obtained for all gemini surfactants with $s \geq 4$. In the presence of 12-2-12 at 2 × cmc, a long-range repulsive interaction that decays exponentially with distance is measured, as is expected for an electrical double-layer interaction. This indicates that both surfaces carry a charge of the same sign. At small separation distances, a steeply repulsive region is observed, beginning at a separation of about 5 nm. A final push through

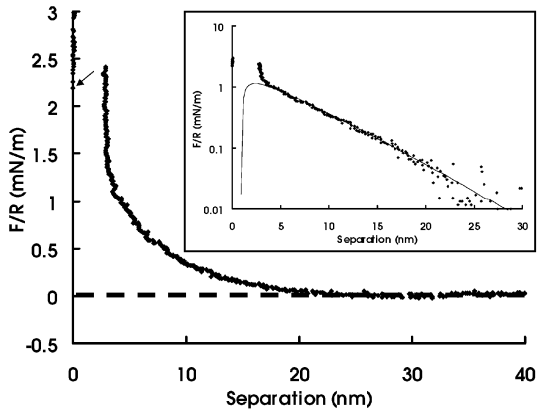

Figure 5. Force versus separation for the interaction of an AFM cantilever probe (Olympus, $R = 1000$ nm, $k = 0.09$ N m^{-1}) with a flat silica substrate immersed in a 1.80 mM aqueous solution of 12-2-12. The data were collected at a pH of 5.9 ± 0.5 and at a constant temperature of 25 ± 0.1 °C. The inset shows a DLVO fit to the same data using the constant-potential boundary condition. ($\Psi_0 = 45$mV, $\kappa^{-1} = 5$ nm. The Hamaker constant used was 0.83×10^{-20} J, which is for silica−water−silica.) Good agreement is obtained down to a separation of 3.5 nm, where the experimental force is greater because of interaction with the adsorbed aggregates.

and jump to contact are then seen at a separation of 3.5 nm. This push-through distance provides a measure of the adsorbed layer thickness described in detail by Wanless and Ducker.[34] This measurement relies upon the surface and the tip experiencing an electrostatic repulsion until, at a specific separation, the tip pushes through the adsorbed layer and makes adhesive contact with the substrate. These data are typical of adsorbed surfactant structures at the solid−liquid interface.[24]

The interaction force measured for 12-12-12 at 2 × cmc has substantially different features from those observed for 12-2-12. A significant long-range repulsive interaction is evident. However, a jump into contact from ∼9 nm is apparent as the gradient of the force exceeds the spring constant. This distance is too large to be attributed to the penetration of the tip through an adsorbed surfactant layer or simple van der Waals forces.

Discussion

Adsorption Isotherms. This study reports the most complete set of adsorption isotherms obtained for gemini surfactants at the silica−aqueous interface, with adsorption isotherms for seven different spacer sizes investigated. The general features of the adsorption isotherms obtained in this study for the most part agree well with those previously reported,[17,18] with the saturation surface excess decreasing with increasing spacer size. However, there are two important differences between the data obtained in this study and those previously reported. First, solution depletion studies show a substantial increase in the surface excess above the solution cmc, an effect that was more pronounced for short spacers. No evidence of this effect was detected in the current study for any spacer length. The isotherms for all spacer lengths reached saturation at or slightly below the solution cmc. The same behavior is found for conventional cationic surfactants adsorbing to silica.[23,30] The cause of the discrepancy between this study and previous studies is unclear. The second discrepancy relates to the concentration required to lead to the second adsorption stage. Previous adsorption isotherms reported that the second adsorption stage for the longest spacer investigated (12-10-12) commenced at lower concentrations than for those with shorter spacer groups. This was attributed to the increased hydrophobicity of the longer chain surfactant. In this study, the concentration leading to the second adsorption step appears to be independent of the spacer length. The difference between the two studies may be related to a change in the ionic strength of the solution upon surfactant adsorption that can occur in depletion studies. Surfactant adsorption to charged surface sites on silica can induce nearby hydroxyl groups to become more acidic.[19] For longer spacer groups, this may result in both headgroups interacting with the substrate and a consequent increase in solution ionic strength.[26] An increased ionic strength will result in the solution cmc being decreased, shifting the features of the adsorption isotherm to lower concentrations. In the experiments reported here using the optical reflectometer, the ionic strength of the solution is unaffected by surface ionization. Gemini surfactants have been noted for their slow exchange kinetics.[10] For all concentrations and all spacer lengths, the adsorption was completed rapidly, within 5 s. The desorption of the geminis was similarly rapid regardless of spacer size.

Surface Coverage. The headgroup area of the gemini surfactants at the air−water interface changes linearly for $2 \leq s \leq 12$. (See Figure 3.) Li et al.[35] have shown that at the air−water interface each gemini surfactant has a charge of 1^+ (i.e., only one of the headgroups is ionized; surface ionization value, $\alpha = 0.5$) regardless of the size of the spacer group. The headgroup area for a conventional ionic surfactant is strongly influenced by electrostatic repulsions; therefore, the headgroup area is expected to be only weakly influenced by the spacer length. Clearly this is not the case. Therefore, we conclude that for the gemini surfactants used here the headgroup area is determined primarily by the *physical size* of the headgroup. This unusual behavior may strongly influence trends in the aggregation behavior of these gemini surfactants.

We have found that the area per molecule at Γ_{max} at the silica−solution interface also changes linearly with spacer group length. This surprising result warrants investigation. Gemini surfactant aggregates in bulk have surface ionization values that vary with spacer length from $\alpha = 0.15$ for $s = 2$, 3, and 4 up to $\alpha = 0.31$ at $s = 12$. (See Table 1.) In comparison, $\alpha = 0.5$ at the air−water interface. Therefore, electrostatic repulsion between headgroups will be *less* important in aggregates than at the air−water interface because of a lower degree of dissociation. Because the headgroup area at the air−water interface is determined by the spacer size rather than electrostatic considerations, we can conclude that the headgroup area in the silica surface aggregates will also be determined by the spacer size. Finally, if the spacer size determines the headgroup area, then for a given gemini of spacer length *s* the headgroup area will be much the same at the air−water interface or within an aggregate.

For cationic surfactants at Γ_{max}, the formation of surface aggregates results in surface-charge reversal and low contact angles indicating the formation of admicelles (bilayered adsorbed structures). Therefore, if a complete bilayer is formed, then the area per molecule at the silica−aqueous interface should be half that of the air−water interface. An evaluation of the experimental data using a patchy bilayer model for the surface aggregates reveals that surface coverage values for all spacer lengths are approximately 40% and are independent of spacer length. (See Table 2.) Therefore, we can conclude that the surface coverage of adsorbed aggregates is similar for all spacer lengths.

Imaging of Aggregates. Images of adsorbed surfactant aggregates of 12-2-12 and 12-3-12 that reveal flattened ellipsoidal structures have been obtained. The adsorption density

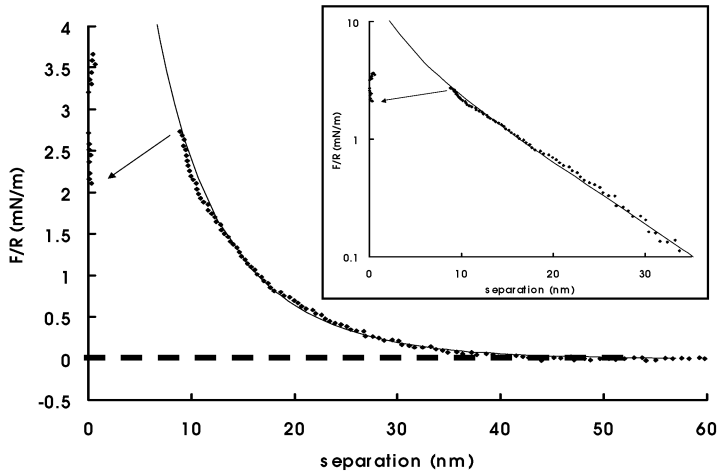

Figure 6. Force versus separation for the interaction of an AFM cantilever probe (Olympus, $R = 1000$ nm, $k = 0.09$ N m^{-1}) with a flat silica substrate immersed in a 0.81 mM aqueous solution of 12-12-12. (The AFM tip and silica substrate were the same as those used for the collection of the data presented in Figure 5.) The data were collected at a pH of 5.9 ± 0.5 and at a constant temperature of 25 ± 0.1 °C. The inset shows a DLVO fit to the same data using the constant-potential boundary condition. ($\Psi_0 = 140$ mV, $\kappa^{-1} = 8$ nm. The Hamaker constant used was 0.83×10^{-20} J, which is for silica−water−silica.) Good agreement is obtained down to a separation of 10 nm, where the experimental force becomes strongly attractive. An attraction of this magnitude at these separations when the surface is hydrophobic is commonly attributed to the long-range hydrophobic attraction.

TABLE 2: Measured and Calculated Characteristics of Adsorbed Gemini Surfactants

spacer length	air−water area/molecule [a] (nm^2)	silica−water area/molecule [b] (nm^2)	surface coverage [c] (%)	aggregation number [d]	aggregate thickness[d] (nm)	proximal desorption (%)
2	0.67	0.601	45	164	3.5	15.0
3	1.05	0.802	38	123	2.68	20.1
4	1.16	0.949	41	104	2.32	23.7
6	1.43	1.178	41	84	1.95	29.5
8	1.76	1.552	44	63	1.54	38.8
10	2.2	1.749	40	56	1.42	43.7
12	2.26	1.954	43	50	1.32	48.9

[a] Reproduced from refs 12 and 13. [b] From Figure 3. [c] Based on a "patchy bilayer" model. [d] The measured Γ_{max} for each gemini is used to determine the aggregation number and aggregate thickness on the basis of a model where the surface coverage and the number of surfactant aggregates per unit area are independent of spacer length. The images of 12-2-12 aggregates are used to determine the aggregate size for $s = 2$. The aggregate size for all other spacer lengths is calculated relative to this. (See Discussion.)

was found to be 150 aggregates per 10 000 nm,^{2} and the aggregate thickness is estimated to be 3.5 nm from the push-through distance obtained from the force curve. The Tanford calculation for the chain length yields 1.67 nm; therefore, the push-through distance is consistent with the presence of admicelles. These surfactants have been shown to form worm-like aggregates in solution. The smaller surface aggregates are due to the influence of the substrate. The physical dimensions and interaggregate spacing of the admicellar structures presented here are similar to those observed for monomeric quaternary ammonium surfactants on silica.[31,36] Obtaining clear images of 12-3-12 was considerably more difficult than for 12-2-12. This is attributed to the decreased adsorption density of 12-3-12. The number of adsorbed molecules of 12-3-12 is 25% lower than that of 12-2-12. As the spacer length increases, the adsorption density continues to fall. Difficulty in imaging surfactant structures corresponding to low surface excess values has been previously reported.[30] Proximal desorption will also make imaging difficult. This is discussed more fully below. For $s > 3$, AFM images of the adsorbed surfactant layer could not be obtained. This is a consequence of the change in the nature of the interaction force between the AFM tip and the surface.

Interaction Forces. Some further insight into the adsorbed layer can be obtained by determining a DLVO theoretical fit for the experimental force curves, as given in the insets of Figures 5 and 6. This cannot be done quantitatively because the tip radius is not independently known. However, the same tip was used for both 12-2-12 and 12-12-12; therefore, an approximate tip radius can be chosen, and qualitative comparisons can be made. The theoretical fit for 12-2-12 is presented as an inset in Figure 5. The theoretical fit and the experimental data are in good agreement, with both data sets exhibiting an exponential electrostatic decay. At a separation of 3.5 nm, the experimental data reveals an additional repulsion that is attributed to physical contact with adsorbed aggregates. The observed surface potential of interaction between the AFM tip and the silica substrate in the presence of 12-2-12 is 45 mV, and the Debye length is 5 nm. When the corresponding fit is performed on the 12-12-12 data (inset Figure 6), a surface potential of 140 mV and a Debye length of 8 nm are required. The Debye lengths required to fit the data will be largely unaffected by any error in the radius of interaction and as such can be used as semiquantitative measures of the ionic strength of the solution. Hence, the degree of ionization of the adsorbed gemini can be inferred. Calculation reveals that for the 12-2-12 50% of the surfactant molecules bear a 2^+ charge. For 12-12-12, 38% of the surfactant molecules bear a 2^+ charge. The Debye length was fitted here using only a 1:1 symmetric electrolyte, and the concentrations were above the cmc. This will introduce an error in the fitted Debye length. Thus, these values should be taken as indicative of the presence of the 2^+ form of the surfactant rather than an accurate representation of

the proportion of the 2^+ form. This demonstrates that a careful study of the measured Debye lengths of a series of gemini surfactants over a range of concentrations should enable the ionization state of the gemini monomers to be determined. This would require the experimental Debye lengths to be fitted using a program that accepts a combination of symmetric (1:1) and asymmetric (2:1) electrolytes. The surface charge of the 12-12-12 surface is approximately five times as great as that of the 12-2-12 surface. An increase in surface charge is expected because in solution the micelle ionization degree increases from $\alpha = 0.15$ at $s = 2$ to $\alpha = 0.31$ at $s = 12$.[26] There is an additional strongly attractive component to the interaction. It is this strong attraction that precludes images of surface aggregates being obtained. What is the origin of this attraction?

Proximal Desorption. It is widely accepted that as surfaces are brought together the surface charge regulates. Within the DLVO framework, the maximum interaction force is bounded by the constant-charge boundary condition, and the minimum interaction force is bounded by the constant-potential boundary condition. The change in adsorption as a function of surface separation is termed proximal desorption. Ducker et al.[37,38] have recently demonstrated that the degree of charge regulation can significantly exceed the constant-potential boundary condition because of short-range hydrophobic interactions, and the magnitude of proximal desorption is significant for cationic surfactants adsorbed to silica surfaces. Furthermore, at concentrations where the surface charge is reversed because of surfactant adsorption, surfactant monomers desorb from the surfaces upon approach to lower the electrostatic repulsion. We have remarked earlier that the adsorption isotherms of the gemini surfactants are somewhat similar to those of CTAB. Subramanian and Ducker have shown that for CTAB concentrations slightly higher than the cmc the proximal desorption increases dramatically at surface separations below 10 nm.[37] At ∼9 nm, the change in adsorption is ∼0.25 molecules per nm^2. If we assume that the adsorption is changing by a similar magnitude in our experiments, then this represents a significant proportion of the total surface excess, up to 50% for the larger spacer groups. (The calculated values are shown in Table 2.) Note that there is a significant decrease in the surface excess with increasing spacer length. Thus, fewer surfactant monomers are required to desorb from the substrate for the longer spacer sizes in order to expose a hydrophobic surface. Additionally, the electrostatic repulsion is greater for the longer spacer lengths; therefore, the driving force for desorption is likely to be greater. Both of these influences strongly suggest that proximal desorption will have a greater effect on the adsorbed structures as the spacer length increases.

The significance of this can be viewed in two ways. First, it is expected that solution-facing monomers will be more likely to desorb from the interface as the tip approaches. As a consequence, a portion of the tail groups of the monomers adsorbed with headgroups facing the silica substrate will be exposed. This will produce hydrophobic surfaces; consequently, the surfaces jump together under the influence of the long-range hydrophobic attraction. Alternatively, the change in proximal desorption itself can be seen to be the origin of the attraction.[37−44] Regardless, it is apparent that significant changes in adsorption may be occurring upon the approach of the tip to the substrate and that this results in an attractive interaction that precludes the imaging of interfacial structures. This process is depicted schematically in Figure 7. The similarity in the force versus distance data obtained for spacer lengths between 4 and 12 leads us to suggest that a similar process is occurring for all of these

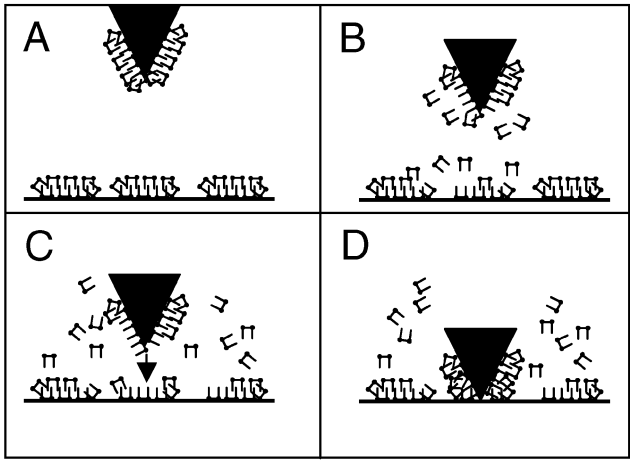

Figure 7. Schematic representation of the diffusion of surfactant molecules out of the adsorbed aggregate on the approach of the AFM tip apex (represented by a large filled triangle) for spacer lengths ≥ 4. The surfactant concentration is sufficient to lead to surface aggregation. No attempt has been made to represent counterions or surfactants that are not adsorbed either at the silica substrate or AFM tip in the first instance, and for simplicity, all surfactants are represented in the cis conformation with straight hydrocarbon chains. (A**)** The tip is far from the interface, at a separation of 30 nm, for example. The AFM senses an electrostatic repulsion, but this repulsion is not sufficient to induce the diffusion of surfactants out of the adsorbed aggregate. **(**B**)** Situation as the AFM tip continues to approach the interface. At these closer separations, the magnitude of the electrostatic interaction is sufficient to force surfactant monomers out of the admicelle. However, the overall electrostatic repulsion is greater than the hydrophobic attraction at these separation distances. **(**C**)** Situation immediately prior to the jump to contact. The outer layer of the surfactant aggregates on both the AFM tip and the substrate has largely diffused into the solution, resulting in the residual electrostatic repulsion being considerably reduced relative to the initial situation and a significant amount of hydrophobe being exposed. The hydrophobic attraction between the surfactant adsorbed to the AFM tip and the substrate leads to the jump to contact observed in the force curve, the magnitude of which is indicated by the arrow. **(**D**)** Expected configuration of surfactant adsorbed to the tip and the substrate in the constant-compliance region. Depending on the stiffness of the adsorbed layer, the AFM tip may push through to contact the silica substrate directly. The situation depicted also leads to the significant adhesion observed for all spacer sizes greater than 3 as the AFM tip is retracted from the substrate.

spacer lengths. Support for this proximal desorption model can be derived from the study of Boschkova et al.,[45] who reported an increase in the frictional properties of the adsorbed layer for 12-*s*-12 gemini surfactants with increasing spacer length.

Despite the difficulty in imaging the adsorbed aggregates for spacers of length greater than 3 we have sufficient information to infer the likely structure of the series of adsorbed aggregates from the images of the 12-2-12 aggregates and the surface excess values. It is known that the same surface excess in terms of the number of monomers is required to neutralize the surface charge for the gemini surfactants.[17] Furthermore, it is generally accepted that surface aggregates form around electrostatically adsorbed monomers.[19−21] Therefore, approximately the same number of surface aggregates should be formed for 12-2-12 up to 12-12-12. This is supported by AFM imaging of the 12-2-12 and 12-3-12 gemini surfactants, which reveals similar numbers of aggregates per unit area despite a 25% difference in the surface excess.

Proposed Structures. Given that the we have the same number of aggregates per unit area and that the surface area occupied by the aggregates does not change with spacer length, by assuming that the mass density of the aggregates does not change we can calculate the aggregate volumes and shapes for

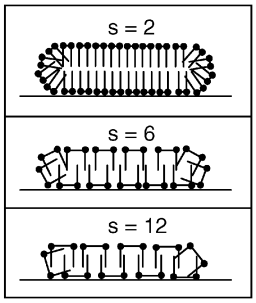

Figure 8. Schematic representation of the variation in the adsorbed surfactant layer as the spacer size is increased. The diagrams presented are 2D cross sections of 3D aggregates present at the interface. Counterions are not represented. The dimensions of the aggregate are similar at all spacer sizes, and it is the increased size of the surfactant headgroup as the spacer length increases that results in lower surface-excess values (and aggregation numbers). Because the adsorbed aggregates cannot be imaged for spacer sizes of 4 or more, the structures depicted are suggested on the basis of area per molecule and force data.

$s > 3$. This is based on what we know of the structure of 12-2-12 aggregates from the images and Γ_{max}. The calculated parameters for the aggregates are shown in Table 2. Clearly, the adsorbed aggregates become more flattened as the spacer length is increased. Schematic representations of the variation in the adsorbed layer structure with spacer length are presented in Figure 8. Clearly, as the headgroup area increases (larger *s*), the surfactant chains interdigitate to a greater degree in order to maximize chain−chain interactions. This leads to the flattening of the aggregate structures.

Conclusions

The equilibrium and dynamic adsorption properties of 12-*s*-12 gemini surfactants at the silica−aqueous interface have been studied using optical reflectometry and atomic force microscopy. Below 0.3 × cmc, the surface excess appears to be independent of the spacer size. At these concentrations, attractive electrostatic interactions between the adsorbed surfactants and the substrate determine the level of adsorption. At increased surfactant concentrations, further adsorption is due to hydrophobic interactions between adsorbed monomers. The saturation surface excess is a function of the spacer size, with the shortest spacer size producing the largest saturation surface excess. The adsorption process is complete within seconds for all spacer sizes at all concentrations.

Soft-contact AFM imaging has revealed flattened ellipsoidal aggregates for $s = 2$ and 3. Images of surfactant aggregates with longer spacer sizes could not be obtained because of an attractive force regime. This attractive force is a consequence of proximal desorption as the AFM tip approaches the substrate. For the longer spacer lengths, the level of proximal desorption is sufficient to disrupt the surface aggregates severely and give rise to a long-range hydrophobic attraction. However, because the area per adsorbed molecule has been shown to vary in a linear fashion with spacer size (over the values of *s* investigated), it can be surmised that similar aggregate geometries are present for all values of *s*.

Acknowledgment. We thank Professor Raoul Zana for donating the gemini surfactants and for his valuable discussions. V.S.J.C. gratefully acknowledges the support of the Australian Research Council.

References and Notes

(1) Deinega, Y. F.; Ul'Berg, Z.; Marochko, L.; Rudi, V.; Denisenko, V. *Kolloidn. Zh.* **1974**, *36*, 649.

(2) Manne, S.; Schaffer, T. E.; Huo, Q.; Hansma, P. K.; Morse, D. E.; Stucky, G. D.; Aksay, I. A. *Langmuir* **1997**, *13*, 6382.

(3) Duval, F. P.; Zana, R.; Warr, G. G. Personal communication.

(4) Menger, F. M.; Littau, C. A. *J. Am. Chem. Soc.* **1993**, *115*, 10083. Dreja, M.; Gramberg, S.; Tieke, B. *Chem. Commun.* **1998**, 1371. De, S.; Aswel, V. K.; Goyal, P. S.; Bhattacharya, S. *J. Phys. Chem. B* **1998**, *102*, 6152.

(5) Zana, R. In *Specialist Surfactant*s; Robb, I. D., Ed.; Chapman Hall Ltd.: London, 1996; Chapter 4, p 81.

(6) Zana, R.; Benrraou, M.; Rueff, R. *Langmuir* **1991**, *7*, 1072.

(7) Danino, D.; Talmon, Y.; Zana, R. *Langmuir* **1995**, *11*, 1448.

(8) Hunter, R. J. *Foundations of Colloid Science*; Oxford University Press: New York, 1985

(9) Rosen, M. J. *Chem. Technol.* **1993**, *23*, 30.

(10) Zana, R. *Curr. Opin. Colloid Interface Sci.* **1996**, *1*, 566.

(11) Zana, R.; Talmon, Y. *Nature (London)* **1993**, *362*, 228.

(12) Espert, A. V.; Klitzing, R.; Poulin, P.; Colin, A.; Zana, R.; Langevin, D. *Langmuir* **1998**, *14*, 1140

(13) Alami, E.; Beinert, G.; Marie, P.; Zana, R. *Langmuir* **1993**, *9*, 1465.

(14) Esumi, K.; Goino, M.; Koide, Y. *J. Colloid Interface Sci.* **1996**, *183*, 539.

(15) Esumi, K.; Takeda, Y.; Goino, M.; Ishiduki, Y.; Koide, Y. *Langmuir* **1997,** *13*, 2585.

(16) Esumi, K.; Uda, S.; Goino, M.; Ishiduki, Y.; Suhara, T.; Fukui, H.; Koide, Y. *Langmuir* **1997**, *13*, 2803.

(17) Chorro, M.; Chorro, C.; Dolladille, O.; Partyka, S.; Zana, R. *J. Colloid Interface Sci.* **1998**, *199*, 169.

(18) Chorro, M.; Chorro, C.; Dolladille, O.; Partyka, S.; Zana, R. *J. Colloid Interface Sci.* **1999**, *210*, 134

(19) Goloub, T. P.; Koopal, L. K.; Bijsterbosch, B. H.; Sidorova, M. P. *Langmuir* **1996**, *12*, 3188.

(20) Goloub, T. P.; Koopal, L. K. *Langmuir* **1997**, *13*, 673.

(21) Atkin, R.; Craig, V. S. J.; Wanless E. J.; Biggs, S. *Adv. Colloid Interface Sci.*, in press.

(22) Eskilsson, K.; Yaminsky, V. V. *Langmuir* **1998**, *14*, 2444.

(23) Atkin, R.; Craig, V. S. J.; Biggs, S. *Langmuir* **2000**, *16*, 9374

(24) *Supramolecular Structure in Confined Geometries*; Manne, S., Warr, G. G., Ed.; ACS Symposium Series 736; American Chemical Society: Washington, DC, 1999.

(25) Zana, R. *J. Colloid Interface Sci.* **2002**, *248*, 203.

(26) Grosmaire L.; Chorro, M.; Chorro, C.; Partyka, S.; Zana, R. *J. Colloid Interface Sci.* **2001**, *243*, 525.

(27) Dijt, J. C.; Cohen Stuart, M. A.; Hofman, J. E.; Fleer, G. J. *Colloids Surf.* **1990**, *51*, 141.

(28) Manne, S.; Cleveland, J. P.; Gaub, H. E.; Stucky, G. D.; Hansma, P. K. *Langmuir* **1994**, *10*, 4409.

(29) Fleming, B. D.; Wanless, E. J. *Microsc. Microanal.* **2000**, *6*, 104.

(30) Atkin, R.; Craig, V. S. J.; Biggs, S. *Langmuir* **2001**, *17*, 6155.

(31) Velegol, S. B.; Fleming, B. D.; Biggs, S.; Wanless, E. J.; Tilton, R. D. *Langmuir* **2000**, *16*, 2548.

(32) Penfold, J.; Staples, E.; Tucker, I. *Langmuir* **2002**, *18*, 2967.

(33) Iler, R. K. *The Chemistry of Silica*; Wiley-Interscience Publishers: New York, 1979.

(34) Wanless E. J.; Ducker, W. A. *J. Phys. Chem.* **1996**, *100*, 3207.

(35) Li, Z. X.; Dong, C. C.; Thomas, R. K. *Langmuir* **1999**, *15*, 4392.

(36) Manne, S.; Gaub, H. E. *Science (Washington, D.C.)* **1995**, *270*, 1480.

(37) Subramanian, V.; Ducker W. A. *J. Phys. Chem. B* **2001**, *105*, 1389.

(38) Lokar, W. J.; Ducker, W. A. *Langmuir* **2002**, *18*, 3167.

(39) Pethica, B. A. *Colloids Surf., A* **1986**, *20*, 151.

(40) Podgornik, R.; Parsegian, V. A. *J. Phys. Chem.* **1995**, *99*, 9491.

(41) Pethica, B. A. *Colloids Surf., A* **1995**, *105*, 257.

(42) Yaminsky, V. V.; Ninham, B. W.; Christenson, H. K.; Pashley, R. M. *Langmuir* **1996**, *12*, 1936.

(43) Yaminsky, V. V.; Jones, C.; Yaminsky, F.; Ninham, B. W. *Langmuir* **1996**, *12*, 3531.

(44) Christenson, H. K.; Yaminsky, V. V. *Colloids Surf., A* **1997**, *129*, 67.

(45) Boschkova, K.; Feiler, A.; Kronberg, B.; Stålgren, J. J. R. *Langmuir* **2002**, *18*, 7930.